LAWRENCE
LIVERMORE
NATIONAL
LABORATORY

LLNL-JRNL-523391

Mechanical deformation of carbon-nanotube-based aerogels

S. J. Shin, S. O. Kucheyev, M. A. Worsley, A. V. Hamza

January 18, 2012

Carbon

Disclaimer

This document was prepared as an account of work sponsored by an agency of the United States government. Neither the United States government nor Lawrence Livermore National Security, LLC, nor any of their employees makes any warranty, expressed or implied, or assumes any legal liability or responsibility for the accuracy, completeness, or usefulness of any information, apparatus, product, or process disclosed, or represents that its use would not infringe privately owned rights. Reference herein to any specific commercial product, process, or service by trade name, trademark, manufacturer, or otherwise does not necessarily constitute or imply its endorsement, recommendation, or favoring by the United States government or Lawrence Livermore National Security, LLC. The views and opinions of authors expressed herein do not necessarily state or reflect those of the United States government or Lawrence Livermore National Security, LLC, and shall not be used for advertising or product endorsement purposes.

Mechanical deformation of carbon-nanotube-based aerogels

S. J. Shin, S. O. Kucheyev, M. A. Worsley, and A. V. Hamza

Lawrence Livermore National Laboratory,

Livermore, California 94551, U.S.A.

(Dated: January 20, 2012)

Abstract

We compare deformation behavior of conventional carbon and carbon-nanotube (CNT) based aerogels with monolith densities of $30-300$ mg cm^{-3}. Results show that CNT-based aerogels have superior elastic moduli, comparable failure stresses, and, hence, lower failure strains. The density scaling law exponents are statistically indistinguishable for both types of aerogels, suggesting the same ligaments connectivity. The superior elastic properties and lower failure strains of CNT-based aerogels are attributed to a higher stiffness of CNT-based ligaments, while comparable failure stresses are attributed to the common junction geometry. Practical implications of these findings are discussed.

Carbon aerogels (CAs) are sol-gel-derived nanoporous carbons, characterized by high electrical and thermal conductivities and a tunable morphology.[1] They can be made as uniform macroscopic monoliths with a wide range of densities down to ~ 10 mg cm^{-3}. Due to such properties, CAs are particularly promising for several energy-related applications, including various electrochemical devices,[2–4] hydrogen storage,[5] catalytic supports,[4,6] energy absorbing structures,[7] compliant electrical contacts,[8] and targets for inertial fusion energy.[9]

Recently, significant effort has been put into designing low-density carbon-nanotube (CNT)-based nanoporous materials[3,7,10–20] with improved properties compared to those of conventional CAs derived from carbonized resorcinol-formaldehyde gels (CRF-CAs). Since many applications of low-density nanoporous solids are limited by their poor mechanical properties, special emphasis has been given to understanding and controlling their deformation behavior.[7,10,12–14,16–18,20] For example, Worsley et al.[14] have reported that composites of CRF-CAs with CNT content of $\gtrsim 16\%$ (that we will refer to below as "CNT-CAs") have a morphology that is very different from the well known string-of-pearls morphology of conventional CRF-CAs.[1,21,22] Ligaments in CNT-CAs are made of CNT bundles, decorated and cross-linked by carbon nanoparticles. Such CNT-CAs have unprecedented, large elastic moduli.[14] The role of CNTs in their elastic behavior is, however, not clear. Is the improvement in the elastic modulus caused by the large stiffness of CNTs or by the different morphology of CNT-CAs compared to that of CRF-CAs? Moreover, while elastic properties of many low-density CNT-based nanofoams have been reported,[7,10,12–14,16–18,20] the often practically more important inelastic deformation behavior of this class of materials remains essentially unexplored.

In this letter, we study mechanical properties of CRF-CAs and CNT-CAs that are closely related to their structure. Our results reveal that the superior elastic properties and lower failure strains of CNT-CAs can be attributed to the high stiffness of CNT-based ligaments, while their failure stresses are dominated by the junction geometry that appears to be the same for both conventional CRF-CAs and CNT-CAs.

The CRF-CAs and CNT-CAs were prepared as described in detail elsewhere.[14] In brief, purified single-walled CNTs (Carbon Solutions, Inc.) were dispersed in water in a sonication bath. The sol-gel precursors (resorcinol and formaldehyde) and the polymerization catalyst ($NaCO_3$) were added, and the mixture gelled. For CRF-CAs, the resorcinol to catalyst molar ratio was fixed to 200. Wet gels were washed with acetone, dried with supercritical

CO_2, and pyrolyzed at 1050 °C under N_2. The final monoliths were machined with a 6-mm-diameter cylindrical endmill rotating at a speed of 2×10^4 revolutions per minute, yielding macroscopically flat surfaces needed for mechanical characterization by indentation.

The samples were indented in the load-controlled mode in an MTS XP nanoindenter with a flat punch diamond tip with an effective diameter of 62 μm. Representative indentation stress (σ) and strain (ε) were defined as $\sigma = 4P/(\pi D^2)$ (i.e., the average contact pressure) and $\varepsilon = (4h)/(\pi D) \approx h/D$ (i.e., the proportionality coefficient between σ and the reduced modulus in the elastic regime).[23,24] Here, P is the load, D is the indenter tip diameter, and h is the indenter displacement. Both loading and unloading rates were kept constant to maintain an indentation strain rate of 10^{-3} s^{-1}.[23]

Figure 1 shows a load–displacement/stress–strain curve, illustrating the parameters that we use to describe the deformation behavior of CRF-CAs and CNT-CAs. All the CAs studied exhibited stress-strain curves qualitatively similar to that of Fig. 1. Loading is characterized by an initial linear-elastic region, followed by a pronounced nonlinear-elastic region, when the shape and volume of the monolith are completely restored after the stress is removed. Failure appears as a sudden jump of the strain at a constant stress (a "pop-in" event). We assign the stress and strain at the initial stage of the first pop-in event as the failure stress (σ^f) and strain (ε^f), respectively.[25] Elastic properties are characterized by the Young's modulus (E), which was calculated based on the initial slope of the unloading curve according to the Oliver-Pharr method[26–28] for maximum loads below those resulting in failure events. For each specimen, several (≥ 4) measurements of E, σ^f, and ε^f were made on different sample locations, and results were averaged. The error bars given are standard deviations.

Figures 2(a)–2(c) show density dependences of mechanical properties (i.e., E, σ^f, and ε^f) of CRF-CAs and CNT-CAs. As mentioned above, when CNT content exceeds $\sim$ 16 wt%, the aerogel morphology drastically changes from the string-of-pearls structure of conventional CRF-CAs to a CNT-CA network of filaments made from CNT bundles decorated and interconnected by carbon nanoparticles.[14,15] It is seen from Fig. 2(a) that this change in the morphology is accompanied by a large (a factor $\sim 2-3$) increase in E. This is in agreement with previous observations.[14]

Figure 2(a) further reveals that moduli of CRF-CAs and CNT-CAs follow statistically indistinguishable scaling laws: $E \propto \rho^{m_E}$, with $m_E \approx 2.5$. This value is consistent with pre-

vious studies of CRF-CAs by Pekala et al.[22] The scaling exponent m_E is determined by ligament connectivity; i.e., how the nanoligaments are interconnected into a three-dimensional structure.[29] For example, the well-known cubic cell model,[29] assuming perfect ligament connectivity, yields an m_E exponent of 2.0. The fact that both CRF-CAs and CNT-CAs have the same m_E values suggests that, even though geometry of ligaments is drastically different, the two structures have similar ligament connectivity.

The enhancement of E for CNT-CAs [Fig. 2(a)] is, therefore, related to a higher stiffness of CNT-based ligaments. Both CRF-CAs and CNT-CAs are made of sp^2-bonded carbon atoms[15] (with $\lesssim$ 10 at.% of H).[30] Since the intrinsic elastic properties of the (partially disordered) graphene sheets forming the ligaments in both CRF-CAs and CNT-CAs are the same, the difference in the ligament stiffness of CRF-CAs and CNT-CAs could be attributed to different ligament geometry. Indeed, for a given density, tubular ligaments of CNT-CAs will have a larger stiffness than rod-like ligaments of CRF-CAs. The two distinct curves in Fig. 2(a), in fact, collapse into one curve when they are plotted as a function of a relative density (i.e., the monolith density normalized to the density of ligaments), with a not unreasonable assumption of densities of graphitic nanoparticles and CNT bundles of 2.2 and 1.3 g cm^{-3}, respectively.[31]

In contrast to full-density solids, failure of inorganic aerogels most likely proceeds through Euler buckling and brittle fracture of ligaments.[23] In this study, the indenter tip contact area (defined by a tip diameter of 62 μm) is much larger than the cross-sectional area of an individual ligament (with a diameter of $\sim$ 20 nm for both CRF-CAs and CNT-CAs),[14,22] making ligament failure a multiple statistical process. Figure 2(b) shows that σ^f remains essentially unaffected by the CNT loading. This suggests that ligament junctions are similar in both types of CAs. Indeed, in CNT-CAs, junctions between CNT-based ligaments are formed by the same interconnected carbon nanoparticles that comprise the ligaments of CRF-CAs. Such graphitic nanoparticles forming ligament junctions are expected to be more defective and, hence, weaker than the CNT bundles themselves, acting as locations of failure events.[32] As a result, both CRF-CAs and CNT-CAs fail when the same critical stress σ^f is applied.

A separation into two distinct curves is observed in Fig. 2(c) for ε^f, with CRF-CAs exhibiting $\sim 2-3$ times larger ε^f values than those of CNT-CAs of the same densities. This is expected given an increased stiffness and similar σ^f for CNT-CAs. For both CNT-CAs

and CRF-CAs, ε^f increases with reducing monolith density. This behavior is consistent with an associated increase in the aspect ratio of nanoligaments with decreasing monolith density.[33]

Figures 2(b) and 2(c) show that power-law fits for σ^f ($\sigma^f \propto \rho^{m_\sigma}$) and ε^f ($\varepsilon^f \propto \rho^{m_\varepsilon}$) give exponents of $m_\sigma \approx 2.0$ and $m_\varepsilon \approx -0.7$ for both CRF-CAs and CNT-CAs, which are also slightly larger than predictions of the cubic cell model ($m_\sigma = 1.5$ and $m_\varepsilon = -0.5$).[29] However, $m_E + m_\varepsilon \approx m_\sigma$, in agreement with what is expected from an elastic fracture behavior.[29]

Results of this work have straightforward implications for selecting and designing nanofoams for a particular application. An independent control of ligament stiffness (e.g., by material selection) and connectivity (e.g., by post-synthesis processing) should be targeted. If low-density monoliths with a high stiffness and failure stress are desired, CNT-CAs are preferred. On the other hand, if the application is limited by the failure strain, conventional CRF-CAs have an advantage over CNT-CAs.

This work was performed under the auspices of the U.S. DOE by LLNL under Contract DE-AC52-07NA27344.

[1] See, for example, a recent review by A. M. Elkhatat and S. A. Al-Muhtaseb, Adv. Mater. **23**, 2887 (2011).

[2] R. W. Pekala, J. C. Farmer, C. T. Alviso, T. D. Tran, S. T. Mayer, J. M. Miller, and B. Dunn, J. Non-Cryst. Sol. **225**, 74 (1998).

[3] T. Bordjiba, M. Mohamedi, and L. H. Dao. Adv. Mater. **20**, 815 (2008).

[4] D. R. Rolison, R. W. Long, J. C. Lytle, A. E. Fischer, C. P. Rhodes, T. M. McEvoy, M. E. Bourga, A. M. Lubers, Chem. Soc. Rev. **38**, 226 (2009).

[5] H. Kabbour, T. F. Baumann, J. H. Satcher, Jr., A. Saulnier, and C. C. Ahn, Source, Chem. Mater. **18**, 6085 (2006).

[6] J. S. King, A. Wittstock, J. Biener, S. O. Kucheyev, Y. M. Wang, T. F. Baumann, S. K. Giri, A. V. Hamza, M. Baeumer, and S. F. Bent, Nano Lett. **8**, 2405 (2008).

[7] A. Cao, P. L. Dickrell, W. G. Sawyer, M. N. Ghasemi-Nejhad, and P. M. Ajayan, Science **310**, 1307 (2005).

[8] G. Toth, J. Malkin, N. Halonen, J. Palosaari, J. Juuti, H. Jantunen, K. Kordas, W. G. Sawyer, R. Vajtai, and P. M. Ajayan, Adv. Mater. **21**, 2054 (2009).

[9] S. O. Kucheyev and A. V. Hamza, Appl. Phys. Rev. **108**, 091101 (2010).

[10] M. B. Bryning, D. E. Milkie, M. F. Islam, L. A. Hough, J. M. Kikkawa, and A. G. Yodh, Adv. Mater. **19**, 661 (2007)

[11] M. A. Worsley, J. H. Satcher, Jr., and T. F. Baumann, Langmuir **24**, 9763 (2008).

[12] S. I. Cha, K. T. Kim, K. H. Lee, C. B. Mo, Y. J. Jeong, and S. H. Hong, Carbon **46**, 482 (2008).

[13] Y. Sato, M. Ootsubo, G. Yamamoto, G. Van Lier, M. Terrones, S. Hashiguchi, H. Kimura, A. Okubo, K. Motomiya, B. Jeyadevan, T. Hashida, and K. Tohji, ACS Nano **2**, 348 (2008).

[14] M. A. Worsley, S. O. Kucheyev, J. H. Satcher, A. V. Hamza, and T. F. Baumann, Appl. Phys. Lett. **94**, 073115 (2009).

[15] M. A. Worsley, P. J. Pauzauskie, S. O. Kucheyev, J. M. Zaug, A. V. Hamza, J. H. Satcher Jr, and T. F. Baumann, Acta Mater. **57**, 5131 (2009).

[16] X. Gui, J. Wei, K. Wang, A. Cao, H. Zhu, Y. Jia, Q. Shu, and D. Wu, Adv. Mater. **22**, 617 (2010); X. Gui, A. Cao, J. Wei, H. Li, Y. Jia, Z. Li, L. Fan, K. Wang, H. Zhu, and D. Wu, ACS Nano **4**, 2320 (2010).

[17] M. Xu, D. N. Futaba, T. Yamada, M. Yumura, and K. Hata, Science **330**, 1364 (2010).

[18] J. Zou, J. Liu, A. S. Karakoti, A. Kumar, D. Joung, Q. Li, S. I. Khondaker, S. Seal, and L. Zhai, ACS Nano **4**, 7293 (2010).

[19] R. R. Kohlmeyer, M. Lor, J. Deng, H. Liu, and J. Chen, Carbon **49**, 2352 (2011).

[20] P. D. Bradford, X. Wang, H. Zhao, and Y. T. Zhu, Carbon **49**, 2834 (2011).

[21] R. W. Pekala, J. Mater. Sci. **24**, 3221 (1989).

[22] R. W. Pekala, C. T. Alviso, and J. D. LeMay, J. Non-Cryst. Solids **125**, 67 (1990).

[23] S. O. Kucheyev, A. V. Hamza, J. H. Satcher Jr, and M. A. Worsley, Acta Mater. **57**, 3472 (2009).

[24] Note that, for flat punch indentation, representative indentation stress and strain are linear functions of the load and indenter penetration, respectively. In the elastic regime, the load–displacement dependence is linear.[23]

[25] Another important observation from Fig. 1 is the energy dissipation in load-unload cycles. This effect will not be discussed here.

[26] W. C. Oliver and G. M. Pharr, J. Mater. Res. **7**, 1564 (1992).

[27] In Oliver-Pharr calculations, we assumed Poisson's ratios of diamond and aerogels of 0.07 and 0.2, respectively, and the Young's modulus of diamond of 1141 GPa.[23,28]

[28] B. Abramoff and L. C. Klein, J. Am. Ceram. Soc. **73**, 3466 (1990).

[29] L. J. Gibson and M. F. Ashby, *Cellular Solids* (Cambridge University Press, Cambridge, 1997).

[30] The elemental composition was measured by a combination of Rutherford backscattering spectrometry (RBS) and elastic recoil detection analysis (ERDA) with 2 and 3 MeV ^{4}He ions, respectively.

[31] Q. Lu, G. Keskar, R. Ciocan, R. Rao, R. B. Mathur, A. M. Rao, and L. L. Larcom, J. Phys. Chem. B **110**, 24371 (2006).

[32] T. A. Schaedler, A. J. Jacobsen, A. Torrents, A. E. Sorensen, J. Lian, J. R. Greer, L. Valdevit, and W. B. Carter, Science **334**, 962 (2011).

[33] S. O. Kucheyev, M. Stadermann, S. J. Shin, J. H. Satcher, Jr., S. A. Gammon, S. A. Letts, T. van Buuren, and A. V. Hamza, Adv. Mater. doi: 10.1002/adma.201103561 (2012).

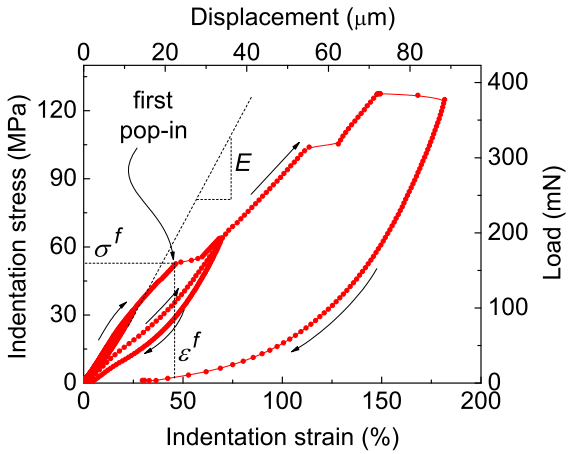

FIG. 1: (Color on-line) Representative load-displacement (stress-strain) curve of a conventional carbon aerogel monolith with a density of 80 mg cm^{-3} indented with a flat punch tip with a diameter of 62 μm. Definitions of the failure strain (ε^f), failure stress (σ^f), and Young's modulus (E) are illustrated. Indentation was performed as a series of loading cycles with increasing maximum loads and complete unloading at the end of each load cycle.

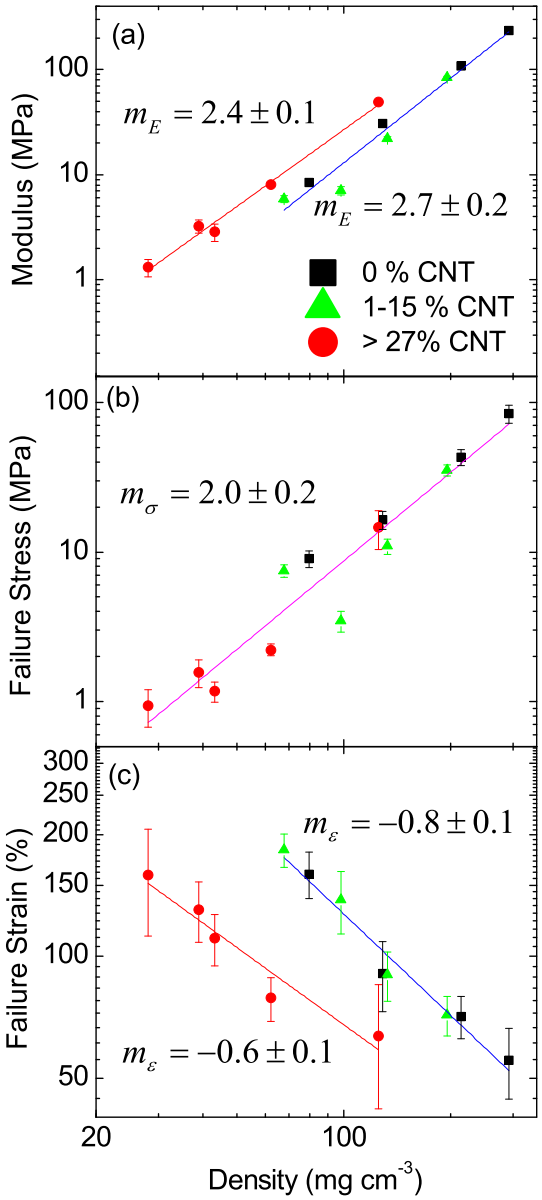

FIG. 2: (Color on-line) Dependence of mechanical properties of carbon aerogels on the monolith density: (a) Young's modulus, (b) failure stress, and (c) failure strain. Solid lines are power-law fits with the exponents indicated.